2024 IEEE/ASME International Conference on Advanced Intelligent Mechatronics (AIM)
July 15-19, 2024. Boston, MA, USA

An Examination of the Thermopiezoelectric Effect in Multilayer Stack Actuators

Rafael Toledo[1], Sascha Eisenträger[2] and Ryan Orszulik[1], *Member, IEEE*

***Abstract*—This paper explores the influence of thermopiezoelectricity in piezoelectric actuators, specifically focusing on multilayer stack actuators. The research aims to investigate the impact of the pyroelectric and electrocaloric effects on the positioning, electric potential, and temperature of these actuators. To accomplish this, a custom finite element code that considers the three fully coupled field equations of thermopiezoelectricity is implemented in MATLAB. In addition, the study is extended to explore the influence that the temperature-dependent piezoelectric strain coefficients have on the stack actuator's behaviour.**

I. Introduction

Piezoelectricity refers to the generation of an electric field when mechanical pressure is applied to a material, or the production of mechanical strain due to an applied electric field. The direct piezoelectric effect occurs when an electric field is generated, and the material behaves as a sensor, while the converse piezoelectric effect occurs when mechanical strain is induced, and the material acts as an actuator [1], [2], [3].

Piezoelectric actuators are commonly used for precision positioning, fine adjustment, and controlled movements in various applications due to their high precision, quick response time, and versatility, making them suitable for a wide range of industries. Additionally, piezoelectric actuators find applications in areas where temperature plays a crucial role, such as in aerospace environments. When the performance of these actuators across a broad range of temperatures must be ensured, the application of the theory thermopiezoelectricity may be required. Thermopiezoelectricity incorporates the thermal field along with the electrical and mechanical fields [4]. Therefore, coupling effects among these three fields, including the pyroelectric and electrocaloric effects, must be considered. The pyroelectric effect generates voltage in response to temperature variations, while the electrocaloric effect produces temperature change due to an applied electric potential.

Numerous studies have developed the theroy of thermopiezoelectricity from different aspects. Mindlin derived the governing equations of linear piezothermoelastic media [5], and Nowacki contributed to the solutions of piezothermoelastic differential equations [6], [7]. Rao and Sunar explored thermopiezoelectric sensors and actuators in intelligent structures using finite element analysis [8]. Görnandt and Gabbert proposed a finite element implementation for solving coupled field problems in thermopiezoelectric smart structures [4]. Ashida and Tauchert investigated thermally-induced wave propagation in piezoelectric plates, considering thermal relaxation time [9]. Tian et al. presented a finite element method for generalized piezothermoelastic problems [10], and a recent study by Baiz et al. focused on a numerical analysis of a piezoelectric contact problem with thermal effects [11].

This paper analyzes the influence of the pyroelectric and electrocaloric effects on multilayer piezoelectric stack actuators. To perform this study, a custom MATLAB finite element code is created that considers the three fully-coupled field equations of thermopiezoelectricity. The analysis is then extended to study the influence of temperature-dependent piezoelectric strain coefficients on the positioning of stack actuators.

II. Linear theory of thermopiezoelectricity

The linear theory of thermopiezoelectricity considers not only the mechanical and electrical fields but also incorporates the thermal field. Thus, the connections amongst these three fields, including both the pyroelectric and electrocaloric effects, need to be taken into account.

Referring to [4], the governing constitutive equations for a thermopiezoelectric material are provided as follows

$$T_{ij} = C_{ijkl}u_{kl} - e_{kij}E_k - \zeta_{ij}\theta \tag{1}$$

$$D_i = e_{ijk}u_{jk} + \varepsilon_{ij}E_j + p_i\theta \tag{2}$$

$$\eta = \zeta_{ij}u_{ij} + p_iE_i + \gamma\theta \tag{3}$$

where T_{ij}, D_i, and η represent the stress tensor, electric displacement, and entropy density, respectively, where tensor index notation has been employed. The parameters C_{ijkl}, e_{kij}, ε_{ij}, and E_i correspond to the elasticity tensor, piezoelectric tensor, dielectric permittivity tensor, and the electric field. The temperature-stress tensor is denoted as ζ_{ij}, and θ represents a temperature change. Therefore, the term $\zeta_{ij}\theta$ in Eq. (1) is referred to as the thermal stress. The pyroelectric tensor is defined as p_i, where the term $p_i\theta$ in Eq. (2) stands for the pyroelectric effect [12], [13]. Further, the term $\zeta_{ij}u_{ij}$ in Eq. (3) represents the heat of deformation (thermal-mechanical coupling), p_iE_i denotes the electrocaloric effect (thermal-electrical coupling effect), and the coefficient γ is expressed as $\rho C_v^E/\Theta_0$, where C_v^E is the specific heat capacity at a constant electric field, and Θ_0 is the reference temperature, representing the point without thermal strain [12], [13], [14].

Given the constitutive thermopiezoelectric equations (Eqs. (1)–(3)) and the presence of three coupled fields (mechanical, electrical, and thermal), the finite element

[1] Rafael Toledo and Ryan Orszulik (ryan.orszulik@lassonde.yorku.ca) are with the Department of Earth and Space Science and Engineering, York University, Toronto, Canada.
[2] Sascha Eisenträger is with the Institute of Mechanics, Otto von Guericke University Magdeburg, Magdeburg, Germany.

formulation can be deduced using the method of weighted residuals (Galerkin's method) as outlined in [4], and can be written as

$$M^e_{uu}\ddot{u}^e + k^e_{uu}u^e + k^e_{u\phi}\phi^e - k^e_{u\theta}\theta^e = f^e_{uu} \tag{4}$$

$$k^e_{\phi u}u^e - k^e_{\phi\phi}\phi^e + k^e_{\phi\theta}\theta^e = f^e_{\phi\phi} \tag{5}$$

$$k^e_{\theta u}\dot{u}^e - k^e_{\theta\phi}\dot{\phi}^e + H^e_{\theta\theta}\dot{\theta}^e + k^e_{\theta\theta}\theta^e = f^e_{\theta\theta} \tag{6}$$

The element mass matrix is given by

$$M^e_{uu} = \int_{V^e} \rho N_u^T N_u dV^e \tag{7}$$

where ρ represents the density, and V^e denotes that the integral is computed across the volume of the element. The stiffness matrix for the mechanical element is expressed as

$$k^e_{uu} = \int_{V^e} B_u^T C B_u dV^e \tag{8}$$

where C represents the elasticity matrix [N/m^2] with dimensions 6×6. In the case of PZT, it adopts the structure of a transversely isotropic material and can be formulated as

$$C = \begin{bmatrix} C^E_{11} & C^E_{12} & C^E_{13} & 0 & 0 & 0 \\ C^E_{12} & C^E_{11} & C^E_{13} & 0 & 0 & 0 \\ C^E_{13} & C^E_{13} & C^E_{33} & 0 & 0 & 0 \\ 0 & 0 & 0 & C^E_{55} & 0 & 0 \\ 0 & 0 & 0 & 0 & C^E_{55} & 0 \\ 0 & 0 & 0 & 0 & 0 & C^E_{66} \end{bmatrix} \tag{9}$$

Here, C^E denotes the elastic constants under a constant electric field. The stiffness matrix for direct piezoelectric coupling is defined as

$$k^e_{u\phi} = \int_{V^e} B_u^T e^T B_\phi dV^e \tag{10}$$

where e stands for the matrix of piezoelectric stress coefficients [N/(Vm)] with dimensions 3×6. In the context of PZT, it can be expressed as

$$e = \begin{bmatrix} 0 & 0 & 0 & 0 & e_{15} & 0 \\ 0 & 0 & 0 & e_{15} & 0 & 0 \\ e_{31} & e_{32} & e_{33} & 0 & 0 & 0 \end{bmatrix} \tag{11}$$

The elasto-thermal element stiffness matrix can be described as follows

$$k^e_{u\theta} = \int_{V^e} B_u^T \zeta N_\theta dV^e \tag{12}$$

where ζ represents the thermal stress coefficient vector [N/(m^{2}K)], derived by multiplying the elasticity (stiffness) matrix C by the vector of thermal expansion coefficients α. The expression for α is provided as

$$\alpha = \begin{bmatrix} \alpha_{11} & \alpha_{22} & \alpha_{33} & 0 & 0 & 0 \end{bmatrix}^T \tag{13}$$

Hence, the thermal stress coefficient vector ζ for PZT can be formulated as

$$\zeta = \begin{bmatrix} C^E_{11}\alpha_{11} + C^E_{12}\alpha_{22} + C^E_{13}\alpha_{33} \\ C^E_{21}\alpha_{11} + C^E_{22}\alpha_{22} + C^E_{23}\alpha_{33} \\ C^E_{31}\alpha_{11} + C^E_{32}\alpha_{22} + C^E_{33}\alpha_{33} \\ 0 \\ 0 \\ 0 \end{bmatrix} \tag{14}$$

The dielectric element stiffness matrix is given as

$$k^e_{\phi\phi} = \int_{V^e} B_\phi^T \varepsilon B_\phi dV^e \tag{15}$$

where ε represents the matrix of dielectric coefficients [F/m] with dimensions 3×3. Its expression is provided as

$$\varepsilon = \begin{bmatrix} \varepsilon^{Tr}_{11} & 0 & 0 \\ 0 & \varepsilon^{Tr}_{22} & 0 \\ 0 & 0 & \varepsilon^{Tr}_{33} \end{bmatrix} \tag{16}$$

where ε^{Tr} denotes dielectric constants measured under free conditions. These are expressed as relative dielectric constants ε multiplied by the permittivity of free space ($\varepsilon_0 \approx 8.8542 \times 10^{-12}$ [F/m]). The stiffness matrix for the pyroelectric element is presented as

$$k^e_{\phi\theta} = \int_{V^e} B_\phi^T p N_\theta dV^e \tag{17}$$

where p represents the vector of pyroelectric coefficients and can be formulated as

$$p = \begin{bmatrix} p_1 & p_2 & p_3 \end{bmatrix}^T \tag{18}$$

The thermal element stiffness matrix is given as

$$k^e_{\theta\theta} = \int_{V^e} B_\theta^T \lambda B_\theta dV^e + \int_{O^e_h} N_\theta^T h_v N_\theta dO^e_h \tag{19}$$

where λ denotes the matrix of heat conduction coefficients [W/(mK)], and its formulation is expressed as

$$\lambda = \begin{bmatrix} \lambda_{11} & 0 & 0 \\ 0 & \lambda_{22} & 0 \\ 0 & 0 & \lambda_{33} \end{bmatrix} \tag{20}$$

The term h_v in Eq. (19), represents the convective heat transfer coefficient over the surface area O^e_h. The formulation for the thermoelastic element stiffness matrix is as follows

$$k^e_{\theta u} = \int_{V^e} N_\theta^T N_\theta \Theta \zeta^T B_u dV^e \tag{21}$$

where Θ denotes the reference temperature. The electrocaloric element stiffness matrix is expressed as

$$k^e_{\theta\phi} = \int_{V^e} N_\theta^T N_\theta \Theta p^T dV^e \tag{22}$$

The stiffness matrix for the heat capacity element is given as

$$H^e_{\theta\theta} = \int_{V^e} N_\theta^T \rho c_v N_\theta dV^e \tag{23}$$

Here, c_v represents the heat capacity coefficient of the material. The external mechanical element force vector is defined as

$$f^e_{uu} = \int_{V^e} N_u^T \rho b dV^e + \int_{O^e} N_u^T \bar{t} dO^e \tag{24}$$

where b stands for the vector of body forces, and O^e represents the surface for which the traction $\bar{t}$ is prescribed. The electric element charge vector is provided as

$$f^e_{\phi\phi} = -\int_{O^e} N_\phi^T \bar{Q} dO^e \tag{25}$$

where $\bar{Q}$ represents the prescribed surface charge on the surface O^e. The external thermal element force vector is formulated as

$$f_{\theta\theta} = \int_{O^e_h} N_\theta^T h_v(\Theta_\infty - \Theta_0) dO^e + \int_{O^e} N_\theta^T \bar{q}_s dO^e + \int_{V^e} \rho r dV^e \tag{26}$$

where Θ_∞ denotes the ambient temperature, $\bar{q}_s$ represents the prescribed heat flux across the surface O^e, and r represents the heat generated by internal sources per unit time. The formation of the matrices involves the application of Gaussian quadrature for evaluation of the integrals. For the sake of simplicity, Eq. (7) demonstrates the Gaussian quadrature technique and is presented as

$$\begin{aligned} M^e_{uu} &= \int_{-1}^{1}\int_{-1}^{1}\int_{-1}^{1} \rho N_u^T N_u |J| d\xi_1 d\xi_2 d\xi_3 \\ &= \sum_{i=1}^{n}\sum_{j=1}^{n}\sum_{k=1}^{n} \rho N_u^T(\xi_i,\xi_j,\xi_k) N_u(\xi_i,\xi_j,\xi_k)|J| W_{\xi_i} W_{\xi_j} W_{\xi_k} \end{aligned} \tag{27}$$

where $|J|$ represents the determinant of the Jacobian matrix.

When the elemental system of differential equations in Eqs. (4–6) is combined into a global matrix, the resulting system of equations can be expressed as

$$\begin{aligned} &\begin{bmatrix} M_{uu} & 0 & 0 \\ 0 & 0 & 0 \\ 0 & 0 & 0 \end{bmatrix} \begin{bmatrix} \ddot{U} \\ \ddot{\Phi} \\ \ddot{\Theta} \end{bmatrix} + \begin{bmatrix} R & 0 & 0 \\ 0 & 0 & 0 \\ K_{\theta u} & -K_{\theta\phi} & H_{\theta\theta} \end{bmatrix} \begin{bmatrix} \dot{U} \\ \dot{\Phi} \\ \dot{\Theta} \end{bmatrix} \\ &+ \begin{bmatrix} K_{uu} & K_{u\phi} & -K_{u\theta} \\ K_{\phi u} & -K_{\phi\phi} & K_{\phi\theta} \\ 0 & 0 & K_{\theta\theta} \end{bmatrix} \begin{bmatrix} U \\ \Phi \\ \Theta \end{bmatrix} = \begin{bmatrix} F_u \\ F_\phi \\ F_\theta \end{bmatrix} \end{aligned} \tag{28}$$

In Eq. (28), the mass M_{uu} of the body is the only term associated with accelerations. In the subsequent term, the damping matrix is introduced, where R denotes the Rayleigh damping matrix commonly utilized in structural dynamics. The third term in the equation, known as the global stiffness matrix, acts on the displacement, electric potential, and temperature and can be used on its own for static analyses. The asymmetry of these two matrices should also be noted. When the first two terms in Eq. (28) are added, dynamic analyses can be performed. The right hand side of the equation constitutes the global force vector, including mechanical, electrical, and thermal forces.

III. Examination of the Thermopiezoelectric Effect in Multilayer Stack Actuators

Piezoelectric stack actuators are multi-layered ceramic actuators that convert electrical energy into longitudinal mechanical displacement with high precision, force, and speed [15], [16]. This section investigates the coupled effects of thermopiezoelectricity based on parameters from a P-887.51 stack actuator from *Physik Instrumente* [15], whose specifications are shown in Table I. The material parameters of the stack actuator P-887.51 are presented in Table II [15].

TABLE I: Specifications for the multilayer stack actuator.

Piezoceramic actuator	P-887.51
Dimensions [mm]	7×7×18
Nominal travel range [µm]	15
Operating voltage [V]	100
Number of layers	375

TABLE II: Material parameters for the multilayer stack actuator.

Parameter	Unit	Value
Compliance matrix	N/m^2	$C = \begin{bmatrix} 1.229\times10^{11} & 7.660\times10^{10} & 7.017\times10^{10} & 0 & 0 & 0 \\ 7.660\times10^{10} & 1.229\times10^{11} & 7.017\times10^{10} & 0 & 0 & 0 \\ 7.017\times10^{10} & 7.017\times10^{10} & 9.705\times10^{10} & 0 & 0 & 0 \\ 0 & 0 & 0 & 2.226\times10^{10} & 0 & 0 \\ 0 & 0 & 0 & 0 & 2.226\times10^{10} & 0 \\ 0 & 0 & 0 & 0 & 0 & 2.315\times10^{10} \end{bmatrix}$
Piezoelectric stress matrix	N/(Vm)	$e = \begin{bmatrix} 0 & 0 & 0 & 0 & 17.735 & 0 \\ 0 & 0 & 0 & 17.735 & 0 & 0 \\ -7.841 & -7.841 & 13.559 & 0 & 0 & 0 \end{bmatrix}$
Dielectric matrix	F/m	$\varepsilon = \begin{bmatrix} 1.638\times10^{-8} & 0 & 0 \\ 0 & 1.638\times10^{-8} & 0 \\ 0 & 0 & 1.550\times10^{-8} \end{bmatrix}$
Mass density	kg/m^3	$\rho = 7800$
Heat conduction matrix	W/(mK)	$\lambda = \begin{bmatrix} 1.1 & 0 & 0 \\ 0 & 1.1 & 0 \\ 0 & 0 & 1.1 \end{bmatrix}$
Thermal expansion matrix	1/K	$\alpha = \begin{bmatrix} 6\times10^{-6} & 6\times10^{-6} & -5\times10^{-6} & 0 & 0 & 0 \end{bmatrix}^T$
Pyroelectric matrix	C/(m^{2}K)	$p = \begin{bmatrix} 0 & 0 & -6\times10^{-4} \end{bmatrix}^T$
Heat capacity coefficient	J/K	$c_v = 350$

A. Step Input Signal

The first study is on the transient analysis of the stack actuator subjected to a step input signal. A realistic model of the stack is created by dividing the actuator into 375 layers, where 100 V and 0 V are alternately applied to the surfaces of each of the layers. Each layer has an opposing polarization orientation to ensure the longitudinal mechanical displacement occurs in the same direction. The stack actuator is discretized with 9375 quadratic (20-node) hexahedral elements, 49596 nodes, and 247980 degrees of freedom, where 148788 degrees of freedom correspond to the mechanical field, and 49596 correspond to the electrical and thermal fields. The simulation is run for 1 second, where the voltage to the stack actuator is a 100 V step input at t = 0.01 seconds and the Newmark method is employed for the solution. The result for the developed displacement over time at the reference node, located at the top of the actuator with original coordinates of (0.0125, 0.005, 0.018) mm, is shown in Fig. 1 for both thermopiezoelectric and piezoelectric simulations. In the piezoelectric simulation, the thermal field is not taken into account. As expected, there is a damped oscillation in the piezoelectric simulation that decays to a constant final position. However, when temperature is incorporated into the analysis, an interesting phenomenon emerges as the actuator's position gradually drifts upward. This drift results in a slight change on the stack position of approximately 11 nm, which could hold significance in nanopositioning applications (see for example [17], [18], [19]), and is qualitatively reminiscent of the creep phenomenon seen in nanopositioning applications.

The underlying reason for the thermopiezoelectric simulation demonstrating a smaller displacement than the piezoelectric simulation lies in the negative thermal expansion coefficient α_3. This coefficient leads to contraction of the stack actuator when subject to temperature with the pyroelectric effect responsible for the upward drift observed in the displacement. This occurs because the developed temperature increases the voltage, subsequently increasing the actuator's displacement.

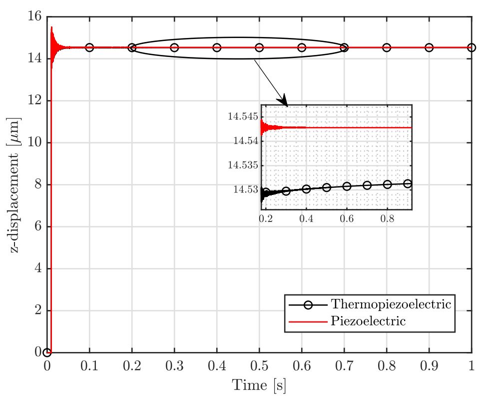

Fig. 1: Comparison of the stack actuator displacement for both thermopiezoelectric and piezoelectric simulations.

Figure 2 presents a cross-sectional xz view of the developed temperature at the step time of 0.01 seconds. This view reveals distinct red and blue regions indicating areas with higher and lower temperatures, respectively. This phenomenon is a result of the pyroelectric coefficient getting switched with the polarization direction in each layer, where one side is the positive terminal, and the other is the negative terminal.

IV. Thermal Load

In contrast to the previous case where a step input was applied, this section investigates the behaviour of the stack actuator under a dynamic thermal load, particularly its impact on the electric potential and position of the actuator. This analysis involves the comparison of two simulations: one considering the pyroelectric effect and the other neglecting it. In these simulations, the top surface of the stack actuator is subjected to a sinusoidal temperature rise with a magnitude of 10 K. The bottom surface maintains a constant temperature of 273.15 K. Boundary conditions are enforced to 0 V alternately on half the surfaces of the actuator, leaving the other half open.

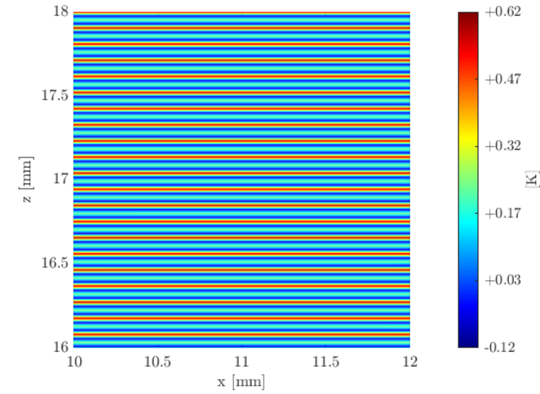

Fig. 2: Side (planar xz) view of the developed temperature in the stack actuator.

Figure 3a demonstrates the resulting displacement and Fig. 3b shows the generated voltage caused by the thermal load. Significant differences are evident between the results that consider the pyroelectric effect and those that neglect it. Specifically, in terms of developed displacement, accounting for the pyroelectric effect yields a result approximately twice as large as that of the simulation that disregards this effect (see Fig. 3a). In Fig. 3b, the developed voltage in the simulation considering the pyroelectric effect is approximately 12.5 times larger than the voltage generated in the simulation that neglects the pyroelectric effect. This significant difference arises from the fact that although three fields are still considered (mechanical, electrical, and thermal), two couplings are missing, the pyroelectric and electrocaloric effects.

V. Temperature Dependence of the Piezoelectric Strain Coefficients

Several studies have measured the temperature dependence of piezoelectric strain coefficients in piezoelectric actuators experimentally [20]. This temperature dependence affects the piezoelectric strain coefficients d_{31} and d_{33} in soft piezoelectric ceramics such as PZT-5A and PZT-5H, which are often used in nanopositioning applications demanding high sensitivity. For stack actuators, the longitudinal strain coefficient d_{33} is more influential, hence this is assumed to be the only temperature-dependent piezoelectric strain coefficient in the simulation.

Up to this point, this paper has assumed that all coefficients are independent of temperature. However, for a more accurate characterization of actuator behavior, the temperature-dependence of the piezoelectric strain coefficient d_{33} must be incorporated at each time step in the transient analysis. To achieve this, the developed code is enhanced by introducing the implementation of the temperature-dependent coefficient

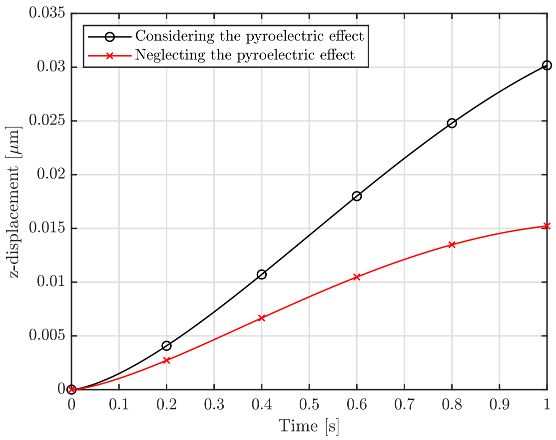

(a) Developed displacement

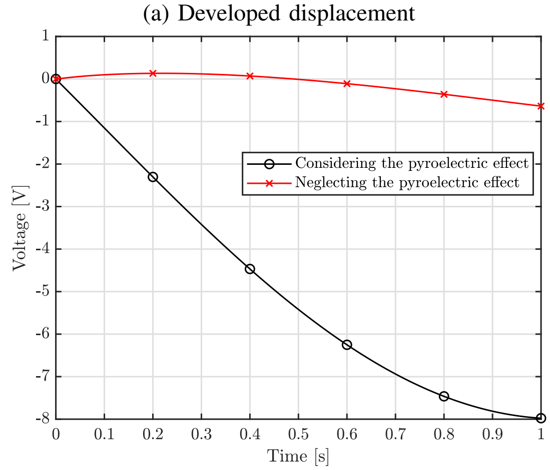

(b) Developed voltage

Fig. 3: Stack actuator under thermal load considering the pyroelectric effect versus neglecting the pyroelectric effect

d_{33}. The algorithm recalculates the piezoelectric strain coefficient d_{33} at each time step by determining the average temperature for each element. Consequently, the updated piezoelectric strain coefficients are employed to find the new element piezoelectric stiffness matrix $k_{u\phi}^e$, and as a result, a block of the global stiffness matrix K is updated at each time step. This process is repeated at every time step of the simulation, making it relatively computationally expensive.

VI. Stack Actuators with Varying Piezoelectric Strain Coefficients Matrix

This section investigates the temperature dependence of the piezoelectric strain coefficient d_{33} in stack actuators. For the stack actuator, this paper works with the coefficients corresponding to PZT-5A, where the coefficient d_{33} is taken to have a value of approximately 400×10^{-12} m/V at a temperature of θ = 20°C. To establish a more accurate relation for the actual d_{33} value (400×10^{-12} m/V), a linear relation for $d_{33}(\theta)$ is assumed up to 100°C as determined experimentally [20]. Consequently, the relationship between the piezoelectric strain coefficient and temperature for PZT-5A can be expressed as $d_{33}(\theta) = 2.615\times10^{-12}\theta + 3.447\times10^{-10}$, as shown in Fig. 4.

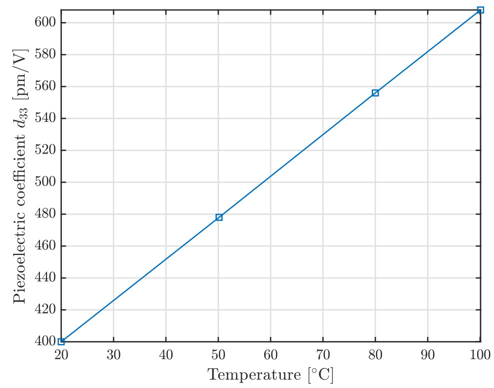

Fig. 4: The assumed temperature dependence of the piezoelectric coefficient d_{33}.

To examine this effect, three simulations are compared: one that considers the piezoelectric effect only, one that considers the thermopiezoelectric effect with a constant piezoelectric strain coefficient, and one that considers the thermopiezoelectric effect with temperature dependence of the d_{33} coefficient. The investigated stack actuator is simplified to a 7-layer model due to the computational time required to recompute (numerically integrate) a block of the global stiffness matrix K at each time step in a 375-layer model. For this case, the stack actuator is discretized with 63 quadratic (20-node) hexahedral elements, 432 nodes, and 2160 degrees of freedom, where 1296 degrees of freedom are corresponding to the mechanical field, and 432 are corresponding to the electrical and thermal fields.

A. Step Input

A step input is applied to alternating surfaces of the stack actuator with the bottom surface of the actuator held at a constant temperature of 273.15 K. The simulation results are presented in Fig. 5, where the simulation considering the temperature-dependent coefficient d_{33} shows a larger developed displacement of approximately 3 nm compared to the piezoelectric simulation, and a larger displacement of approximately 13 nm compared to the thermopiezoelectric simulation with constant piezoelectric strain coefficients. This behavior is expected since the temperature dependence of the coefficient d_{33} linearly increases, meaning that the change in temperature causes the piezoelectric coefficient to become larger. The piezoelectric simulation produces a larger displacement than the thermopiezoelectric simulation with a constant d_{33} coefficient, a difference of approximately 10 nm. This result is due to the negative α_3 coefficient, which causes the actuator to contract. As a result, this contraction leads to a slightly smaller displacement in the thermopiezoelectric simulation that has a constant coefficient d_{33}.

VII. Conclusion

This paper presented the development of a MATLAB-based finite element code designed to numerically solve the fully-coupled field equations of thermopiezoelectricity. The

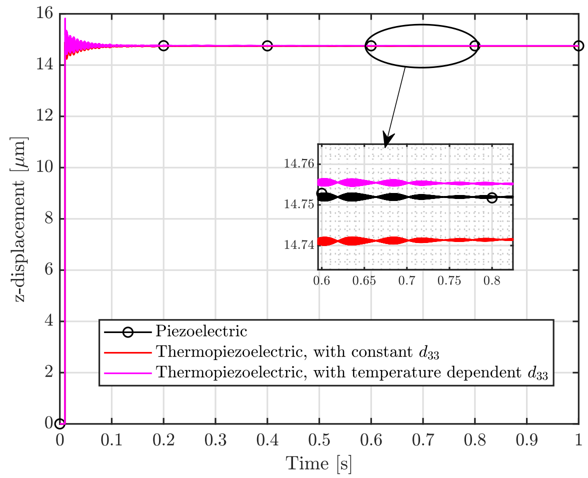

Fig. 5: Time versus developed actuator displacement for the three considered cases.

primary objective was to explore the impacts of pyroelectric and electrocaloric effects on multilayer stack piezoelectric actuators, along with their temperature dependence. The response to an applied voltage step input was analyzed comparing thermopiezoelectric and piezoeletric simulations. In the thermopiezoelectric simulation, it was observed that the z-displacement exhibited a gradual increase over time due to the pyroelectric effect. In contrast, the piezoelectric simulations showed a constant z-displacement after the decay of the initial transient response, resulting in a difference of approximately 11 nm. Furthermore, another dynamic analysis was carried out for a time-varying thermal load. The multilayer stack actuator was subjected to a temperature increase, and in this scenario, the voltage and z-displacement were examined for simulations that considered and neglected the pyroelectric effect. The findings revealed that the pyroelectric effect exerted a significant influence on the developed displacement (approximately twice as large in simulations accounting for the pyroelectric effect) and on the voltage (approximately 12.5 times larger in simulations accounting for the pyroelectric effect). These discrepancies are significant and emphasize the importance of considering the pyroelectric effect in applications with large variations in the thermal environment.

Lastly, a simplified model was used to conduct an investigation on the effect of the temperature-dependent piezoelectric strain coefficient d_{33}. A step voltage input was investigated for three models: piezoelectric, thermopiezoelectric with constant d_{33}, and thermopiezoelectric with temperature dependent d_{33}. As expected, the model with a temperature-dependent coefficient yielded a larger displacement than the other simulations due the fact that the piezoelectric strain coefficient increases with the produced temperature. This difference was of approximately 13 nm when compared to the thermopiezoelectric simulation with constant coefficient d_{33}. In future work, incorporation of the dependence of the piezoelectric strain coefficient on the electric field strength should also be considered along with a physically motivated hysteresis model.

References

[1] K. Uchino, *Advanced Piezoelectric Materials: Science and Technology*, 1st ed., Woodhead Publishing, 2010.

[2] J. Tichi, *Fundamentals of Piezoelectric Sensorics: Mechanical, Dielectric, and Thermodynamical Properties of Piezoelectric Materials*, Springer, 2010.

[3] P. Dineva, D. Gross, R. Müller, and T. Rangelov, *Piezoelectric Materials*, Springer International Publishing, 2014, pp. 7–32.

[4] A. Görnandt and U. Gabbert, "Finite element analysis of thermopiezoelectric smart structures," *Acta Mechanica*, vol. 154, no. 1, pp. 129–140, 2002. [Online]. Available: https://doi.org/10.1007/BF01170703

[5] R. Mindlin, "Equations of high frequency vibrations of thermopiezoelectric crystal plates," *International Journal of Solids and Structures*, vol. 10, no. 6, pp. 625–637, 1974. [Online]. Available: https://www.sciencedirect.com/science/article/pii/002076837490047X

[6] W. Nowacki, "Some general theorems of thermopiezoelectricity," *Journal of Thermal Stresses*, vol. 1, no. 2, pp. 171–182, 1978.

[7] J. P. Nowacki, "Steady-state problems of thermopiezoelectricity," *Journal of Thermal Stresses*, vol. 5, no. 2, pp. 183–194, 1982.

[8] S. Rao and M. Sunar, "Analysis of distributed thermopiezoelectric sensors and actuators inadvanced intelligent structures," *AIAA Journal*, vol. 31, no. 7, pp. 1280–1286, 1993.

[9] F. Ashida and T. R. Tauchert, "Thermally-induced wave propagation in a piezoelectric plate," *Acta Mechanica*, vol. 161, pp. 1–16, 2003.

[10] X. Tian, J. Zhang, S. Yapeng, and T. Lu, "Finite element method for generalized piezothermoelastic problems," *International Journal of Solids and Structures*, vol. 44, pp. 6330–6339, 2007.

[11] A. Oultou, O. Baiz, and H. Benais, "Numerical analysis of a piezoelectric contact problem with locking material and thermal effects," *Discrete and Continuous Dynamical Systems - Series S, AIMS*, pp. 1–20, 2023.

[12] P. Li, F. Jin, and J. Ma, "Mechanical analysis on extensional and flexural deformations of a thermo-piezoelectric crystal beam with rectangular cross section," *European Journal of Mechanics*, vol. 55, pp. 35–44, 2016. [Online]. Available: https://www.sciencedirect.com/science/article/pii/S0997753815001047

[13] R. Mindlin, "High frequency vibrations of piezoelectric crystal plates," *International Journal of Solids and Structures*, vol. 8, no. 7, pp. 895–906, 1972. [Online]. Available: https://www.sciencedirect.com/science/article/pii/0020768372900042

[14] H. J. Lee, "Finite element analysis of active and sensory thermopiezoelectric composite materials," PhD Thesis, National Aeronautics and Space Administration, Glenn Research Center, Cleveland, OH United States, 2001. [Online]. Available: http://purl.access.gpo.gov/GPO/LPS26899

[15] P. Ceramics, "Piezoelectric actuators." [Online]. Available: https://www.piceramic.com/en/

[16] C. Niezrecki, D. Brei, S. Balakrishnan, and A. Moskalik, "Piezoelectric Actuation: State of the Art," *The Shock and Vibration Digest*, vol. 33, pp. 269–280, 2001.

[17] D. Xu, Y. Liu, J. Liu, X. Yang, and W. Chen, "Developments of a piezoelectric actuator with nano-positioning ability operated in bending modes," *Ceramics International*, vol. 43, pp. S21–S26, 2017. [Online]. Available: https://www.sciencedirect.com/science/article/pii/S0272884217310143

[18] R. R. Orszulik, F. Duvigneau, and U. Gabbert, "Dynamic modeling with feedforward/feedback control design for a three degree of freedom piezoelectric nanopositioning platform," *Journal of Intelligent Material Systems and Structures*, vol. 29, no. 3, pp. 301–309, 2018. [Online]. Available: https://doi.org/10.1177/1045389X17704063

[19] G. Y. Gu, L. M. Zhu, C. Y. Su, and H. Ding, "Motion Control of Piezoelectric Positioning Stages: Modeling, Controller Design, and Experimental Evaluation," *IEEE/ASME Transactions on Mechatronics*, vol. 18, no. 5, pp. 1459–1471, 2013.

[20] Z. Dapeng, J. Qinghui, and L. Yingwei, "The effect of temperature and loading frequency on the converse piezoelectric response of soft PZT ceramics," *Materials Research Express*, vol. 4, no. 12, pp. 125 705–8, 2017. [Online]. Available: https://dx.doi.org/10.1088/2053-1591/aa9dbc